Finite Element Analysis on Magnetic and Mechanical Characteristics for Hybrid Magnetic Bearing

Hou Eryong
Institute of Aerospace Technology
College of Aerospace Science and Engineering, National University of Defense Technology
Changsha, China
houeryong1@163.com, houeryong@nudt.edu.cn

Liu Kun
Institute of Aerospace Technology
College of Aerospace Science and Engineering, National University of Defense Technology
Changsha, China
liukun@nudt.edu.cn

***Abstract*—The configuration and working principle of a novel radial hybrid magnetic bearing (RHMB) are introduced in this paper, and its 3-D nonlinear finite element model, based on which air gap magnetic field distributions and magnetic forces on the rotor under different displacements and control currents are calculated, is established with the software ANSYS. The magnetic forces calculated by finite element method (FEM) are compared with those calculated by equivalent magnetic circuit method. The results show that the FEM can comprehensively reflect the magnetic field distribution and mechanical characteristics for the RHMB. When the rotor is in a suspension state without a static load or external disturbance, the air gap magnetic field is uniform and continuous, which is advantageous in reducing eddy current loss. The fluxes of the two radial channels are decoupled from each other, which is favor of reducing control power loss and simplifying control algorithm of the system. The radial magnetic force is approximately linear with respect to radial displacement and control current under the premise that soft magnetic material is not saturated, which is advantageous in improving system control precision. The thrust bearings in conventional structures could be excluded because of the axial passive resilience and large passive stiffness in the novel RHMB, which makes the system a low power loss and a simple structure.**

Keywords-finite element; hybrid magnetic bearing; magnetic field distribution; mechanical characteristic

I. INTRODUCTION

Hybrid magnetic bearings (HMBs) depend on several permanent magnets to provide bias fluxes and on several coils to provide control fluxes. They have the merit of low loss and can realize passive suspension in several degrees of freedom compared with active magnetic bearings, and have a better controllability on stiffness and dampness compared with passive magnetic bearings. Therefore, HMBs have been widely used in many fields, such as aerospace and energy [1]-[3]. To reduce eddy current loss and enhance load capacity of the existing HMBs, a novel radial HMB (RHMB) is proposed in [4].

Magnetic field distribution is one of the most important items for magnetic bearing design, but is usually very difficult to measure because of the small air gap length. Load capacity and stiffness, which are important indexes of magnetic bearings and mainly determines their performances and applications, are nonlinear functions of rotor displacement and control current. Nowadays, magnetic field calculation and structural design mainly depend on the equivalent magnetic circuit method [5]-[7], in which reluctances and nonlinearities of soft magnetic materials and the effects of leakage flux, fringing, eddy current, and hysteresis are ignored, and the magnetic potential is considered to dropping all on working air gaps. Obviously, the equivalent magnetic circuit method cannot obtain the exact magnetic field distribution and has a low precision in calculating load capacity and stiffness because of too many assumptions and simplifications. To enhance load-capacity-to-mass ratio of magnetic bearings, it is sometimes necessary to use some soft magnetic materials of high saturation flux density to make bearings work in their nonlinear intervals. At this time, the linear models obtained by the equivalent magnetic circuit method are usually unsatisfactory. Besides, magnetic force is obviously nonlinear with respect to a large rotor displacement or control current and then the approximate linear model can not comprehensively reflect their actual relationships. Therefore, it is indispensable to thoroughly research the characteristics of magnetic bearings by a field method which is more accurate than the equivalent magnetic circuit one. Finite element method (FEM) is one of the commonly used numerical tools in field methods. Finite element models are much more close to their physical prototype than the mathematical models obtained by the equivalent magnetic circuit method. Therefore, more accurate results of magnetic field distribution and magnetic force can be obtained by the FEM.

Knight et al. researched a C-shaped magnetic bearing by nonlinear FEM and calculated its magnetic force by the principle of virtual work [8]. In the same way, the influence of bearing geometric parameters on radial magnetic force is analyzed in [9], and the current stiffness and displacement stiffness are calculated and compared with the linearized bearing parameters in [10]. The magnetic field and leakage flux distributions of a thrust bearing are analyzed in [11]. The leaf element is expanded into the edge FEM to calculate the eddy current losses in the thin surface layer of a laminated core [12]. The 3-D finite element models are used to calculate the magnetic field distribution and the force-displacement and the force-current characteristics [13]-[16]. The results are compared with those of the equivalent magnetic circuit method

and some prototypes are designed in [15]-[16]. The 2-D transient FEM are used to analyze the influences of eddy current, leakage flux, fringing, and flux saturation on bearing dynamic performances [17]. The load capacity and stiffness results calculated by both the 2-D and the 3-D FEMs are in good agreement with those of experiment [18]-[19]. In this paper, the 3-D finite element model of the RHMB is established, and the air gap magnetic field distributions and mechanical characteristics for different displacements and currents are calculated to show light on the advantages of the RHMB and the FEM.

II. Configuration and Working Principle

The novel RHMB belongs to the four-pole homopolar structure and its configuration and flux paths are shown in Fig. 1, wherein the solid lines with arrows represent the paths of bias fluxes, which are generated by several permanent magnets, and the dotted lines with arrows represent the paths of control fluxes, which are generated by several coils. All permanent magnets of the four poles are axially magnetized in a same axial direction. There are eight coils in all, four of which are used in the control of translation in the X direction, the other four in the control of translation in the Y direction. The main structural parameters of the RHMB are shown in Table I.

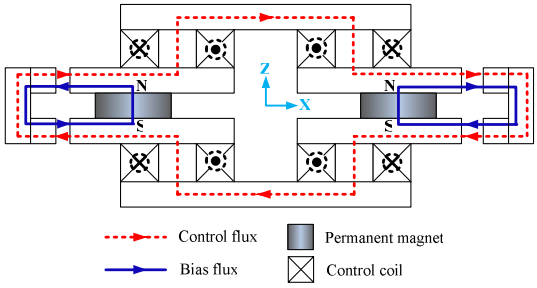

Fig. 1. Configuration and flux paths of the RHMB.

TABLE I. Structural Parameters of the RHMB

Parameter	Value
Length of the air gap /mm	0.71
Inner diameter of the rotor /mm	80.96
Height of the magnetic pole board /mm	4
Height of the permanent magnet/mm	4
Turns of the coil	141

When there is no external disturbance, the rotor locates at its equilibrium position and no current flows through the coils. When the rotor is disturbed to move from the equilibrium position, the offset detected by the displacement sensors is transferred to the controller and then converted to a control signal according to a predefined control law to adjust the control current of the coils. The fluxes generated by the control current are added to the bias fluxes in the air gaps of a larger length and subtracted from the bias fluxes in the opposite air gaps. Then, the rotor is drawn back to its equilibrium position by the resultant force generated by the magnetic fields of the two sides.

III. Finite Element Model

The 3-D finite element model of the RHMB is established with the software ANSYS and shown in Fig. 2. The four stator poles in conventional RHMBs are connected with four connecting channels into a magnetic pole board, shown as Fig. 2 (b). The connecting channels between the neighbor poles for a same magnetic pole board can easily be saturated because of its small sectional area, which makes the fluxes of neighbor poles be independent of each other. At the same time, the connecting channels make the discrete air gaps of conventional RHMBs to be two hollow cylinders, the upper and the lower air paps, shown as Fig. 2 (c). The arrows in Fig. 2 (d) denote the positive directions of each coil. The four coils in a same channel are connected in series with the controller into a closed loop.

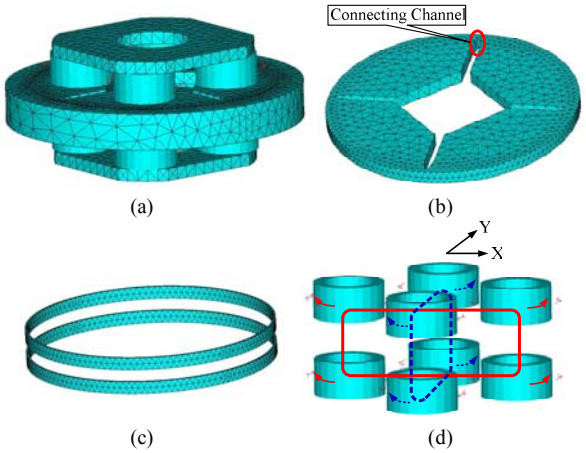

Fig. 2 3D finite element models of (a) the RHMB, (b) the magnetic pole board, (c) the air gaps, and (d) the coils.

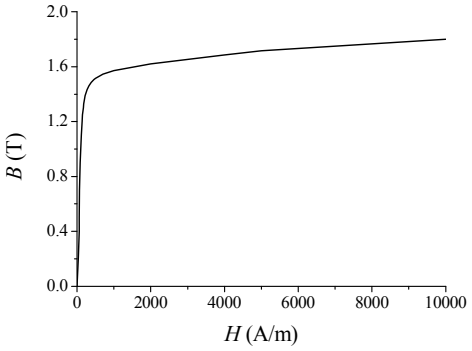

Fig. 3. *B-H* curve of the DT4C.

Considering the influence of leakage flux, the model of the RHMB is surrounded with several air elements, which are not shown in Fig. 2. The permanent magnets are made from rare earth Sm-Co, whose demagnetization curve is approximated to be a straight line, and is defined by the parameters H_c and μ_r in the ANSYS. The other components are made of pure electric iron DT4C, which is defined by the nonlinear *B-H* curve in Fig. 3 considering the influence of magnetic saturation. The 3-D model of the RHMB consists of 81403 nodes, 59274 SOLID98 elements, and 8 SOURC36 elements (coils). The volumes for air gaps are refined to improve computational precision.

IV. MAGNETIC FIELD DISTRIBUTIONS

In this section, the magnetic field distribution of the RHMB is analyzed for three different states, namely, equilibrium, suspension, and eccentric states, classified according to the magnitude of rotor displacement. In equilibrium state, the rotor does not have any displacement, the centers of the rotor and the stator are coincident (x=0, y=0, where x and y are the displacement components in the X and Y directions, respectively), and the air gap lengths everywhere are the nominal value δ_0. In suspension state, the rotor displacement is no more than a critical value determined by a certain application requirement. In this paper, the critical value is 10 μm according to the control precision of a reaction flywheel. The eccentric state refers to the circumstances that the rotor displacement is range from 10 μm to its maximum, which is the air gap length between touchdown bearings and the rotor.

A. Equilibrium State

When the rotor is in its equilibrium position, the air gap flux density distributions for different control currents i_x are calculated and shown in Fig. 4, wherein the circumferential angle of abscissa starts from the +X axis, taking clockwise direction as positive. When there is no static load or external disturbance on the rotor, no current flows through the coils and only bias fluxes flow through the air gaps. Therefore, the air gap flux densities are almost identical and equal to a constant B_0. The vector plots of the flux density in the upper and the lower air gaps are shown in Fig. 5, respectively. The upper air gap flux densities, whose directions are along the exterior normals of the air gap, are similar to the lower air gap ones in magnitude but opposite in direction.

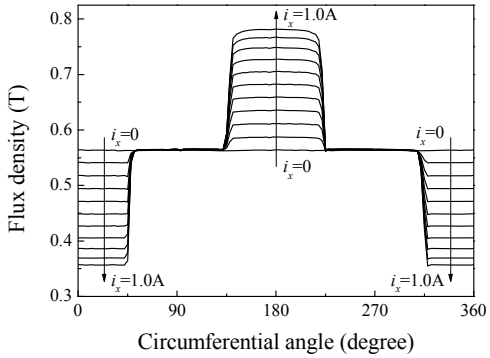

Fig. 4. Air gap flux densities versus circumferential angle for different control currents i_x in equilibrium state when i_y=0.

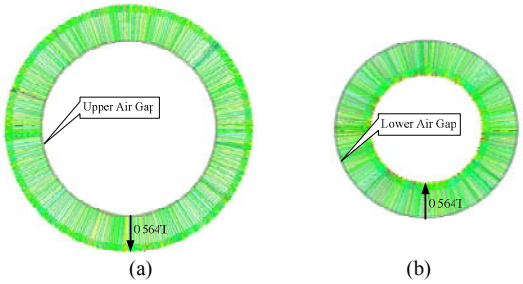

Fig. 5. Vector plots of flux densities for (a) the upper air gap and (b) the lower air gap when i_x=0, i_y=0.

When the rotor is acted by a static load or external disturbance, a proper control current is indispensable to maintain the equilibrium state. When a positive current is applied to the X channel, the air gap flux densities of the Y channel are also B_0, while those of the +X pole ($0°<\theta<45°$ & $315°<\theta<360°$, where θ is the circumferential angle) decrease and those of the –X pole ($135°<\theta<225°$) increase. However, the air gap flux densities of the four poles are also uniformly distributed in their own poles, respectively. At this moment, a resultant force in the +X direction is produced by the air gap magnetic field. The RHMB has the largest load capacity in theory among the analogous bearings because its magnetic pole central angle has reached the maximum 90° of the four-pole structures. When i_x=1.0 A, i_y=0, the flux density vector plot of the upper magnetic pole board is shown in Fig. 6. The control fluxes are added to the bias fluxes and the magnetic potential is increased in the –X pole, which makes a few fluxes flow from the –X pole to the +Y ($225°<\theta<315°$) and the –Y ($45°<\theta<135°$) poles via the connecting channels A (θ=225°) and B (θ=135°), respectively. In contrast, the magnetic potential is decreased in the +X pole, and a few fluxes flow from the +Y and the –Y poles to the +X pole via the connecting channels D (θ=315°) and C (θ=45°), respectively. The connecting channels can be saturated by a very few fluxes because of their small sectional areas, just as that in Fig. 6 the flux densities of the connecting channels have a maximum 1.87 T, which makes the fluxes of neighbor poles be independent of each other.

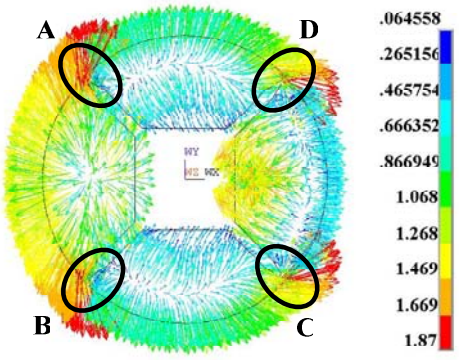

Fig. 6. Flux density vector plot of the upper magnetic pole board when i_x=1.0 A, i_y=0.

B. Suspension State

In fact, it is impossible to control the rotor being in the equilibrium state and the rotor displacement is usually controlled in a certain range according the requirement of precision. In other words, the RHMB is mostly in the suspension state. When x=10 μm, y=0, i_y=0, the air gap flux density distributions for different control currents i_x are calculated and shown in Fig. 7, from which it can be seen that the air gap flux density distributions have few variation compared with those in the equilibrium state. When there is no static load or external disturbance on the rotor, just a very small current is needed to maintain the suspension state and the air gap flux density distributions are also uniform, which can greatly reduce the eddy current losses when the rotor runs and is especially significant for high-speed applications.

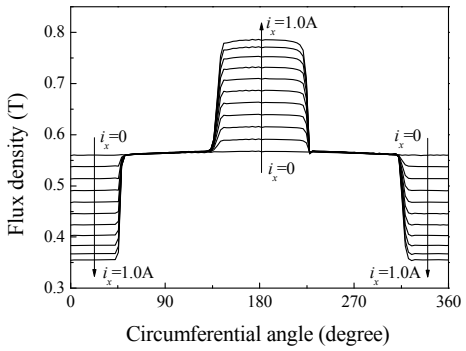

Fig. 7. Air gap flux densities versus circumferential angle for different control currents i_x in suspension state when x=10 μm, y=0, i_y=0.

C. *Eccentric State*

The air gap flux density distributions for different control currents i_x in three eccentric states are calculated and shown in Fig. 8. It can be seen from Fig. 8 (a) that the +X air gap flux densities are smaller than the –X air gap flux densities because of the +X rotor displacement when i_x=0. Then a resultant force in the +X direction is produced by the bias fluxes. After a positive current i_x is applied, the +X air gap flux densities decrease while the –X air gap flux densities increase, which increases the resultant force and makes the rotor offset more. Therefore, this case is actually meaningless. The increment of the air gap flux density is lesser when i_x increases from 0.9 to 1.0 A because the magnetic pole board in the –X direction has been in its nonlinear interval (B>1.4 T), shown as Fig. 9.

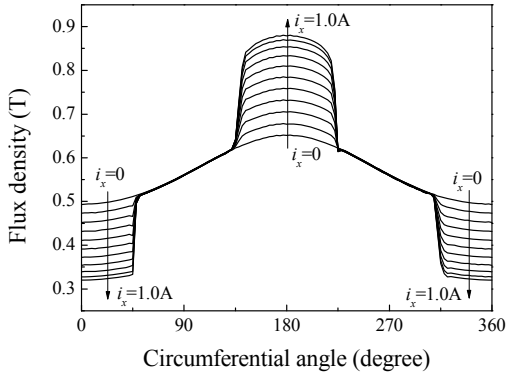

(a)

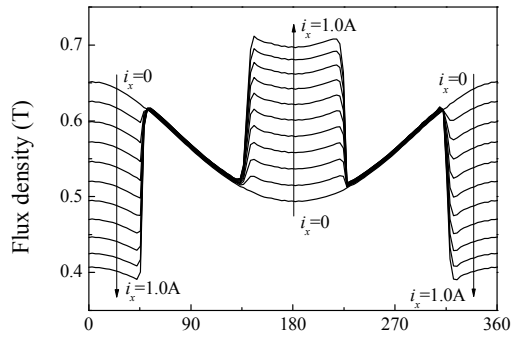

(b)

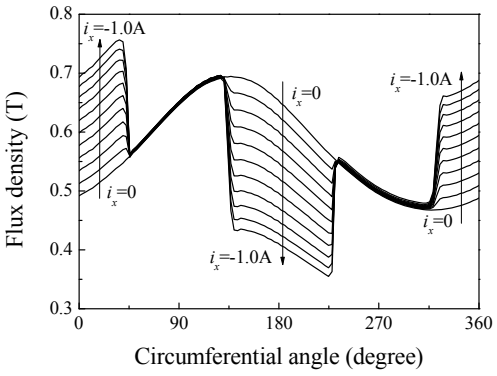

(c)

Fig. 8. Air gap flux densities versus circumferential angle for different control currents i_x in eccentric state when (a) x=0.1 mm, y=0, i_y=0, (b) x=–0.1 mm, y=0, i_y=0, and (c) x=0.1 mm, y=0.1 mm, i_y=0.

The resultant force generated by the bias fluxes on the rotor is in the –X direction when the rotor offsets along the –X direction. It can be seen from Fig. 8 (b) that when a positive current i_x is applied, the +X air gap flux densities decrease while the –X air gap flux densities increase. When the current i_x is larger than a critical value (about 0.3 A), the magnetic force generated by the –X air gap fluxes is larger than that generated by the +X air gap fluxes, i.e., the direction of the resultant force is converted, and then the rotor is drawn back to its equilibrium position. That is just the working principle of the RHMB.

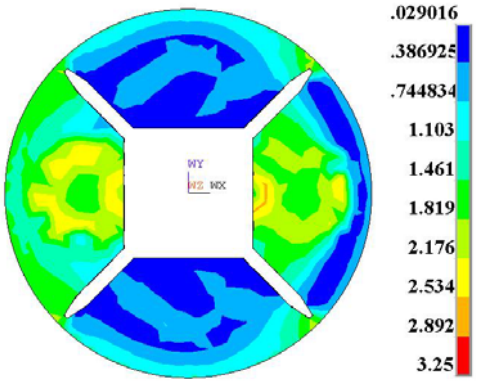

Fig. 9. Flux density contour plot of the upper magnetic pole board when x=–0.1 mm, y=0, i_x=1.0 A, i_y=0.

It can be seen from Fig. 8 (c) that when x=0.1 mm, y=0.1 mm, i_x=0, i_y=0, the air gap flux densities have their maximum in the channel B and minimum in the channel D. According to the previous analysis and Fig. 8 (c), the rotor offset in the X direction can be eliminated by applying a sufficient control current i_x, while the variations of flux density distributions in the Y channel are too slight to be ignored.

In Figs. 8 (b) and (c), the air gap flux densities in the Y direction have a slight variation because of the flux magnitude and direction changes in the connecting channels with the increase of i_x. For instance, in Fig. 8 (b), the flux in channel C flows from the +X pole to the –Y pole when i_x=0, decreases and finally flows from the –Y pole to the +X pole with the increase of i_x.

Based on an overall consideration of Figs. 8 (a), (b) and (c), it can be concluded that whether there is an offset or not in the Y direction, the control current applied to the X channel has no notable influence on the air gap flux density distribution of the Y channel. In other words, the fluxes of the two radial channels for the novel RHMB are decoupled from each other, which is advantageous in reducing control power loss, simplifying control algorithm, and improving control precision.

V. MECHANICAL CHARACTERISTICS

Based on the analysis of last section, the force-current and force-displacement characteristics are analyzed in this section, taking X channel as an example because of the structural symmetry and the flux decoupling of the two radial channels.

A. Force-Current Characteristic

When y=0, i_y=0, the relationships between radial magnetic force f_x and control current i_x for different displacements x (–0.1, 0 and 0.1 mm) are calculated and compared with the results of the equivalent magnetic circuit method, shown as Fig. 10. It can be seen from Fig. 10 that when i_x is small, f_x is directly proportional with respect to i_x, the current stiffness in equilibrium state is 86.93 N/A, and the force results of the FEM and the equivalent magnetic circuit method are in good agreement with each other. The results of the two methods are greatly inconsistent with each other when i_x is large. The force f_x calculated by the equivalent magnetic circuit method is markedly nonlinear with respect to i_x, while that calculated by the FEM is also linear with respect to i_x. Taking x=0 for instance, $|f_x|$ increases slowly with $|i_x|$ when $|i_x|$>0.9 A, *i.e.*, the current stiffness is very small. This is because that the four coil irons of the X channel have been saturated, shown as Fig. 11. According to Fig. 10, the linear interval of i_x for the force-current is about from –0.9 to 0.9 A because the displacement is very small in the suspension state. To raise material utilization ratio, the common design principle for HMBs is that when the load capacity reaches its maximum, the coil irons and the magnetic pole boards are simultaneously saturated, just as that in Fig. 11 the –X pole of the upper magnetic pole board is about to be saturated. Therefore, to enhance the load capacity, the areas of the coil irons and the magnetic poles should be simultaneously enlarged.

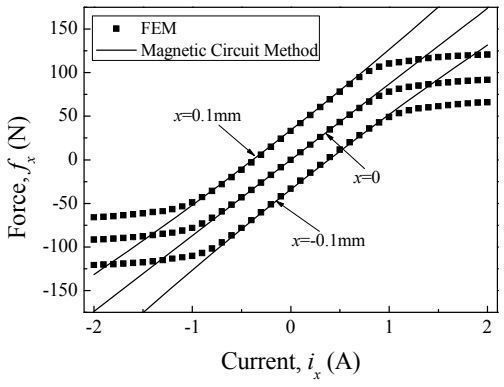

Fig. 10. Relationships between radial magnetic force and control current for different x when y=0, i_y=0.

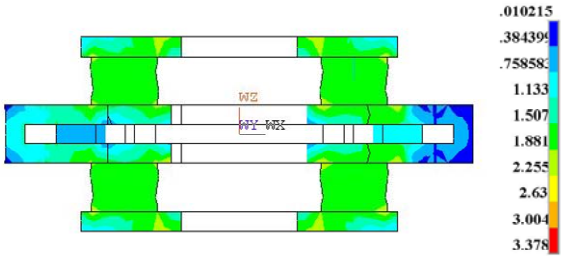

Fig. 11. Contour plot of flux density distribution for the RHMB when x=0, y=0, i_x=1.0 A, i_y=0.

B. Force-Displacement Characteristic

When y=0, i_y=0, the relationships between radial magnetic force f_x and displacement x for different currents i_x (–0.2, 0 and 0.2 A) are calculated and compared with the results of the equivalent magnetic circuit method, shown as Fig. 12, from which it can be seen that the results of the FEM and the equivalent magnetic circuit method are in good agreement with each other within the clearance space. The radial magnetic force f_x is approximately linear with respect to the displacement x and the displacement stiffness is 2.56×10^5 N/m in the equilibrium state.

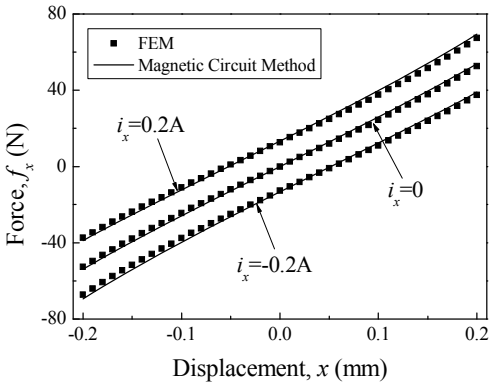

Fig. 12. Relationships between radial magnetic force and displacement for different i_x when y=0, i_y=0.

When there is no radial displacement on the rotor or current in the coils, the relationship between axial magnetic force f_z and displacement z is calculated and shown in Fig. 13. It can be seen from Fig. 13 that $|f_z|$ increases with $|z|$, and f_z and z are always in the opposite directions, which indicate that when there is an axial displacement on the rotor, an axial passive resilience generated by the RHMB itself can draw the rotor back to its equilibrium position. However, the axial passive stiffness decreases with the increase of $|z|$. When $|z|$<0.4 mm, f_z is approximately linear with respect to z and the axial passive stiffness is -4.7×10^4 N/m. The axial passive stiffness of the RHMB is larger than those of conventional homopolar HMBs such as that in [13] with a same stator radius because of its large magnetic pole central angle. The thrust bearings in the conventional HMBs can be excluded for the systems with a low requirement in axial load capacity and control precision, which can simplify the structure and control system, and reduce the power loss and weight.

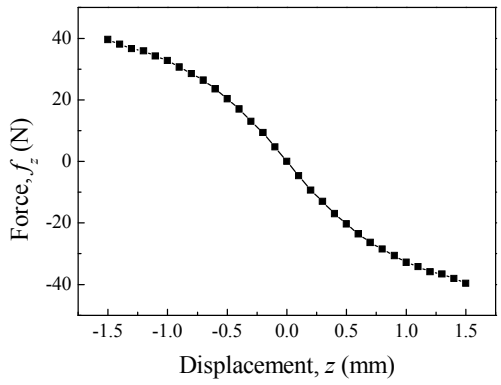

Fig. 13. Relationship between axial magnetic force and displacement when x=0, y=0, i_x=0, i_y=0.

VI. CONCLUSIONS

The magnetic field distributions and mechanical characteristics of a novel RHMB are calculated by the FEM in this paper and some conclusions are obtained and summarized as follows:

(1) Its air gap magnetic field is uniform and continuous when it is in the working order, which is advantageous in reducing eddy current loss.

(2) The fluxes of the two radial channels are decoupled from each other, which is advantageous in reducing control power loss, simplifying control algorithm, and improving control precision.

(3) Its radial magnetic force is linear with respect to the radial displacement and control current, which is also advantageous in improving control precision.

(4) Its axial passive resilience is approximately linear with respect to the axial displacement and its axial passive stiffness is larger than those of the conventional homopolar HMBs.

(5) The results calculated by the FEM, an efficient analysis and design mean for magnetic bearings can comprehensively reflect the magnetic and mechanical characteristics of the RHMB because of the considered leakage flux and material nonlinearity.

REFERENCES

[1] S. Jinji and F. Jiancheng, "A novel structure of permanent magnet biased radial hybrid magnetic bearing," J. Magn. Magn. Mater., vol. 232, no. 2, pp. 202–208, Jan. 2011.

[2] F. Jiancheng, S. Jinji, X. Yanliang, and W. Xi, "A new structure for permanent-magnet-biased axial hybrid magnetic bearings," IEEE Trans. Magn., vol. 45, no. 12, pp. 5319–5325, Dec. 2009.

[3] M. A. Pichot and M. D. Driga, "Loss reduction strategies in design of magnetic bearing actuators for vehicle applications," IEEE Trans. Magn., vol. 41, no. 1, pp. 492–496, Jan. 2005.

[4] H. Eryong and L. Kun, "A novel structure for low-loss radial hybrid magnetic bearing," IEEE Trans. Magn., (2011), doi: 10. 1109/TMAG. 2011. 2160649.

[5] H. Bangcheng, "Modeling and analysis of novel integrated radial hybrid magnetic bearing for magnetic bearing reaction wheel," Chin. J. Mech. Eng., vol. 23, no. 5, pp. 655–662, May 2010.

[6] M. H. Kimman, H. H. Langen, and R. H. M. Schmidt, "A miniature milling spindle with active magnetic bearings," Mechatronics, vol. 20, no. 2, pp. 224–235, Mar. 2010.

[7] M. Hofer, E. Schmidt, and M. Schrödl, "Design of a three phase permanent magnet biased radial active magnetic bearing regarding a position sensorless control," in 24th Annual IEEE Applied Power Electronics Conf. and Expo., Washington, D.C., USA, Feb. 2009, pp. 1716–1721.

[8] J. Knight, Z. Xia and E. McCaul, "Determination of forces in a magnetic bearing actuator: numerical computation with comparison to experiment," Trans. ASME, J. tribol, vol. 114, pp. 796–801, 1994.

[9] F. Z. Hsiao and A. C. Lee, "An investigation of the characteristic of electromagnetic bearings using the finite element method," Trans. ASME, J. tribol, vol. 116, pp. 710–719, 1994.

[10] H. Bangcheng, L. Yefan, J. Hongguang and W. Yihui, "Calculation of forces of radial active magnetic bearing using finite element method," Tribology, vol. 24, no. 2, pp. 160-163, 2004.

[11] L. Shuqin, X. Hua, C. Jianrong and Y. Lie, "Analysis of electromagnetic field for thrust electromagnetic bearings," Tribology, vol. 20, no. 1, pp. 42-45, 2000.

[12] K. Muramatsu, T. Shimizu, A. Kameari, I. Yanagisawa, S. Tokura, O. Saito, et al., "Analysis of eddy currents in surface layer of laminated core in magnetic bearing system using leaf edge elements," IEEE Trans. Magn., vol. 42, no. 4, pp. 883–886, Apr. 2006.

[13] X. Yanliang, D. Yueqin, W. Xiuhe and K. Yu, "Analysis of hybrid magnetic bearing with a permanent magnet in the rotor by FEM," IEEE Trans. Magn., vol. 42, no. 4, pp. 1363–1366, Apr. 2006.

[14] L. Yong, L. Wei and L. Yongping, "Computer-aided simulation analysis of a novel structure hybrid magnetic bearing," IEEE Trans. Magn., vol. 44, no. 10, pp. 2283–2287, Oct. 2008.

[15] F. Jiancheng, S. Jinji, X. Yanliang, and W. Xi, "A new structure for permanent-magnet-biased axial hybrid magnetic bearings," IEEE Trans. Magn., vol. 45, no. 12, pp. 5319–5325, Dec. 2009.

[16] F. Jiancheng, S. Jinji, L. Hu, and T. Jiqiang, "A novel 3-DOF axial hybrid magnetic bearing," IEEE Trans. Magn., vol. 46, no. 12, pp. 4034–4045, Dec. 2010.

[17] S. Yanhua, H. Yick-Sing, and Y. Lie, "Dynamic stiffnesses of active magnetic thrust bearing including eddy-current effects," IEEE Trans. Magn., vol. 45, no. 1, pp. 139–149, Jan. 2009.

[18] T. M. Lim, D. S. Zhang, J. J. Yang, S. B. Cheng, S. H. Low, L. P. Chua, et al., "Design and parameter estimation of hybrid magnetic bearings for blood pump applications," Mech. Syst. Signal Pr., vol. 23, no. 7, pp. 2352–2382, Oct. 2009.

[19] W. K. S. Khoo, K. Kalita, S. D. Garvey, R. J. Hill-Cottingham, D. Rodger, and J. Fred Eastham, "Active axial-magnetomotive force parallel-airgap serial flux magnetic bearings," IEEE Trans. Magn., vol. 46, no. 7, pp. 2596–2602, Jul. 2010.